IEEE Access
Multidisciplinary | Rapid Review | Open Access Journal

Received August 10, 2019, accepted September 12, 2019, date of publication October 1, 2019, date of current version November 8, 2019.

Digital Object Identifier 10.1109/ACCESS.2019.2944950

Comparative Study on Chaos Identification of Ionospheric Clutter From HFSWR

LYU ZHE[1], YU CHANGJUN[1], LIU AIJUN[1], YANG XUGUANG[2], AND QUAN TAIFAN[1]

[1]Harbin Institute of Technology, Weihai 264200, China
[2]School of Information Engineering, Long Dong University, Qingyang 745000, China

Corresponding author: Yu Changjun (yuchangjun@hit.edu.cn)

This work was supported in part by the National Natural Science Foundation of China under Grant 61571159, Grant 61571157, and Grant 61801141.

ABSTRACT In addition to target echoes, high frequency surface wave radar (HFSWR) receives sea and ionospheric clutter. Among these clutters, the ionospheric clutter is dominant and significantly affects the detection performance of HFSWR, particularly when the targets are located 100 kilometers away from the radar, rendering it an unsolved problem for HFSWR. Existing studies concerning HFSWR ionospheric clutter lack empirical research on the nonlinear dynamical characteristics of the ionosphere of HFSWR as existing ionospheric suppression methods are still insufficient to adapt the project application. Therefore, the present study utilized the threshold segmentation method to eliminate the sea clutter in HFSWR Range-Doppler spectrum and extracted ionospheric signals from this spectrum by edge feature extraction. Subsequently, the chaotic invariants, such as correlation dimension and the largest Lyapunov exponent of HFSWR ionospheric clutter, were calculated by phase space reconstruction, whilst the chaotic dynamical characteristics of HFSWR ionospheric clutter were determined by the 0-1 test for chaos and other algorithms. Furthermore, the present study demonstrated, for the first time, the chaotic dynamics of the ionospheric clutter of HFSWR with a low-dimensional attractor by processing and analyzing the experimental data from the Weihai High Frequency Radar Station. The conclusion redefines HFSWR ionospheric clutter based on chaotic dynamics rather than regarding it as a stochastic process, which is conducive to efforts to explore the formation mechanism of ionospheric clutter in essence, which can ultimately improve the detection capability of HFSWR, particularly for long-distance targets.

INDEX TERMS High frequency surface wave radar, ionosphere, chaos, nonlinear dynamical systems.

I. INTRODUCTION

For decades, the high frequency surface wave radar (HFSWR) has been widely used for the detection of targets above the horizon (including offshore vessels and low-flying aircrafts) and sea state remote sensing (ocean currents, wind direction and wave height) [1]. The echoes of HFSWR consist of sea clutter, ionospheric clutter and various types of noise including environment noise, industrial noise and frequency modulation (FM) broadcasting. Various forms of characteristics analysis and suppression methods have been widely studied and adopted in the field of sea clutter research [2]–[4], yet the study of ionospheric clutter is still in the exploration stage. In particular, the present study refers to the small amount of radiation which is reflected by the ionosphere as ionospheric clutter in accordance with HFSWR-related literature [5].

The most intuitive and prominent feature of ionospheric clutter in HFSWR is the stratified structure in the Range-Doppler spectrum. High frequency electromagnetic waves can be reflected by the E-layer, F-layer and expanding layer. The reflection from different layers has specific characteristics. In general, the echoes reflected from the E-layer are concentrated in the range dimension and the expansion in the Doppler dimension occupies small areas [6] and [7]. The ionospheric clutter reflected by the F-layer occupies more cells in the range and Doppler dimension than the E-layer, which persists longer than the E-layer and the spatial correlation of the F-layer is resilient. With regards to the expanding E- and F-layer which habitually exists between 90 and 400 kilometers, the ionospheric clutter from the expanding layer has an impact on the detection performance

The associate editor coordinating the review of this manuscript and approving it for publication was Guolong Cui.

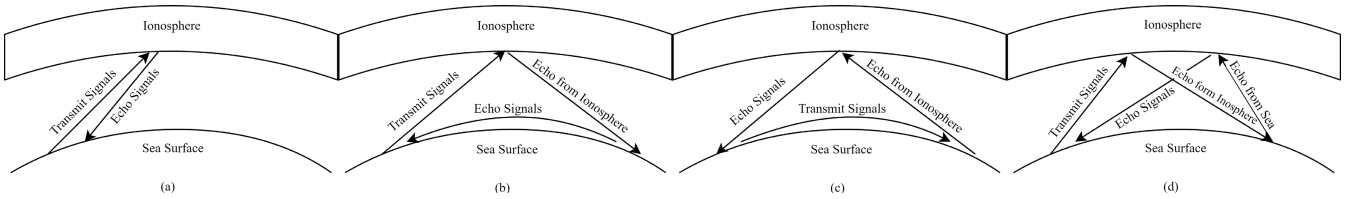

FIGURE 1. Propagation path of ionospheric clutter: (a) once reflection directly by ionosphere; (b) reflection by ionosphere and then propagation along sea surface; (c) propagation along sea surface and then reflection by ionosphere; (d) twice reflection by ionosphere.

of HFSWR because this segment of ionospheric clutter has extensive expansion in the range and Doppler dimension, which coincides with the radar detection power region [8].

The modeling of ionospheric clutter is a extensively studied problem in HFSWR. The majority of the modeling theories of ionospheric clutter are focused on establishing the mathematical models of ionospheric echoes. Chen *et al.* [9] derives an ionospheric clutter power model for vertical reflection, and it is confirmed that the vertical ionospheric plasma drift velocity results in a Doppler shift in the Range-Doppler spectrum. In addition, the vertical ionospheric clutter power model is developed to adopt the sky-sea mixed-path propagation, and explains that how the ionosphere velocities, wavelengths and wind directions on the surface of the sea affect the power spectrum in the mixed-path propagation [10]. The existing literature [11] and [12] has proposed similar analytical models. Moreover, research has derived an expression for the first- and second-order received electric field after a single scatter from the sky-sea mixed paths. Ravan [13] also introduced an ionospheric model based on path integrals of ray-tracing equations which was proposed to forecast the power spectrum of ionospheric echoes reflected by the irregularities in the plasma.Thus, this model is used to simulate three-dimensional space-time-range radar data cubes [14]. Li [15] demonstrated an ionospheric clutter model concerning only the E-layer and, based on this model, a suppression method in HFSWR was exposed. However, these theoretical models have seldom been examined directly using actual experimental data. Furthermore, the mathematical basis of these models is sourced from Barrick [2] and [3] the sea clutter Bragg model, yet sea and ionospheric clutter are distinct physical processes. The ionospheric clutter formation process is significantly more complex than that of the sea clutter.

In addition, several studies [16]–[18] suggest that ionospheric clutter is a stochastic process. The statistical analysis of ionospheric clutter in HFSWR indicates that approximately 90 percent of the ionospheric clutter pertains to the Rayleigh distribution, and the other satisfies the Weibull distribution. The correlation of ionospheric clutter in adjoining range cells is clearly observed [16]. Additionally, the author demonstrates that the ionospheric clutter satisfies the normal distribution when the ionosphere is in the weak fluctuation state [17]. One study analyzed the DOA of ionospheric clutter and suggested that there were significant diversities in ionospheric clutter from various directions of arrival. It is apparent that the ionospheric clutter in HFSWR has high time-varying, statistical and strong spatial-correlation characteristics [18].

The present study acknowledges that a novel approach is required for the mechanism of ionospheric clutter in HFSWR, which is a nonlinear dynamical method. One of the principal aims is to determine whether the ionospheric clutter in HFSWR is a chaotic dynamical process. The present study will compare results from various chaotic identification methods. Meanwhile, the chaotic characteristics of ionospheric clutter will be analyzed. The key contribution of the present study is that it provides a new perspective for studying the characteristics of ionospheric clutter in HFSWR, which has symbolic benefits in terms of suppression methods of ionospheric clutter.

II. IONOSPHERIC CLUTTER IN HFSWR

In particular, the existing ionospheric clutter suppression methods [19] to [20] are far removed from the actual system requirements. The main cause of this unsatisfactory result can be clarified from two central aspects.

Firstly, the radio wave propagation path is extremely complex in HFSWR. There are primarily four paths of ionospheric echoes from the transmitter to the receiver, namely one reflection, sky-sea mixed path, sea-sky mixed path and two reflections, as shown in Figure1. Different paths of reflection result in varied displays in the Range-Doppler spectrum after the two-dimensional Fourier transform. Figure2(a) and (b) show the typical Range-Doppler spectrum of multi-path effects due to different propagation paths.

Secondly, the physical state of the ionosphere is extremely unstable. The ionosphere is the ionized part of the Earth upper atmosphere from approximately 60 to 1,000 kilometers in altitude, a region that includes the thermosphere as well as sections of the mesosphere and exosphere. According to the variation in electron density and altitude, the ionosphere can be approximately apportioned into the D-layer (60 to 90 kilometers), E-layer (90 to 140 kilometers), F-layer (90 to 400 kilometers) and outer atmosphere (equal to and exceeding 400 kilometers). The ionosphere is actively influenced by solar radiation, season, longitude and latitude as well as day and night [1]. Therefore, high-frequency electromagnetic waves are refracted, reflected and modulated as they traverse the varying ionosphere, resulting in the complex display on the Range-Doppler spectrum. As shown

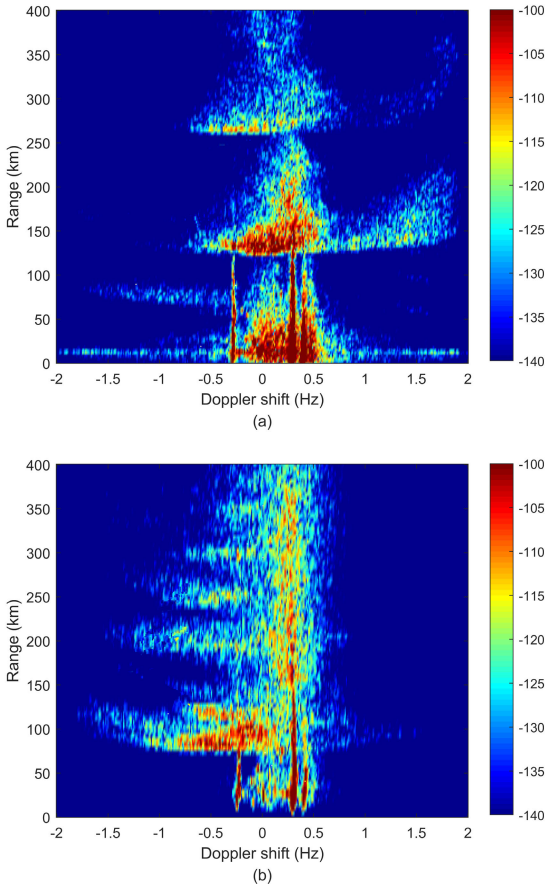

FIGURE 2. Multipath effect of ionospheric clutter: (a) Range-Doppler spectrum of twice multipath effect of ionospheric clutter, (b) Range-Doppler spectrum of multiple multipath effect of ionospheric clutter.

TABLE 1. Basic information about the experimental database.

Parameters	Values
Working frequency	4.1MHz
Pulse repetition period	3.45ms
Pulse duration	0.45ms
Range resolution	0.45km
Sampling frequency	400kHz
Experiment data	2019.01

in Figures3(a) to (d), there is standard ionospheric clutter in HFSWR including the E-layer, F-layer, expanding E- and F-layer clutter.

A. INFORMATION CONCERNING HFSWR

The database in the present study is sourced from the Weihai High Frequency Radar Station, China. The surface wave radar system consists of transmitter and transmitting antennas, receiver and receiving antennas, a signal processor, a situation displaying and spectrum monitoring system. The outer experimental environment is shown in Figure4, and the remote and display system is shown in Figure5. The basic information concerning the database in this experiment is shown in Table1.

B. ABSTRACTED IONOSPHERIC DATA

The Range-Doppler spectrum of HFSWR mainly consists of detections signals, sea clutter and ionosphere clutter [21]. The performance of ionospheric clutter in the Range-Doppler spectrum is different from that of other echo signals, which has a number of characteristics. Firstly, as the ionospheric D-layer cannot reflect the high frequency electro-magnetic wave, ionospheric clutter is usually located beyond 90kilometers in the range dimension. Secondly, ionospheric clutter usually appears as a band or sheet in the Range-Doppler spectrum. If the Range-Doppler spectrum is viewed as a color image, the sea clutter appears as two slim ridges and the target signal echoes appear as a point. It was determined that ionospheric clutter is clearly different from the point targets and sea clutter in the Range-Doppler spectrum. Therefore, the Range-Doppler color spectrum can be considered as image processing and subsequently, ionospheric clutter can be detected by image segmentation technology. In the process of segmentation, the method of image edge extraction is adopted. The extraction process is shown in Figure6.

The primary concern is the position of the ionospheric clutter in the range dimension of the Range-Doppler spectrum. Thus, the Range-Doppler spectrum can be divided into two segments, namely the existence and the absence of ionospheric clutter. Thereafter, the frequency domain data can be converted into time domain data using an inverse Fourier transform. Taking Figure3(a) as example, the most significant step is to extract the outline of the ionospheric clutter in the Range-Doppler spectrum, and the result is shown in the Figure7. In Figure7(b), it is observed that the ionospheric clutter occupies the range cells from 100 to 350 kilometers.

C. IONOSPHERIC TIME DOMAIN DATA

According to Takens' theorem [21], a chaotic dynamical system can be reconstructed from a time sequence of observations of the state. The time delay embedding method is the most typical algorithm to reconstruct the phase-space. Presuming that the ionospheric clutter time series is $X = x_1, x_2, \ldots, x_n$ and reconstruct phase-space in an m-dimension is reconstructed. The state-space multivariate vector R^m assigns the coordinates as:

$$R^m = \begin{bmatrix} X_1 \\ X_2 \\ \vdots \\ X_{N+(m-1)\tau} \end{bmatrix} = \begin{bmatrix} x_1 & x_{1+\tau} & \cdots & x_{1+(m-1)\tau} \\ x_2 & x_{2+\tau} & \cdots & x_{2+(m-1)\tau} \\ \vdots & \vdots & \ddots & \vdots \\ x_N & x_{N+\tau} & \cdots & x_{N+(m-1)\tau} \end{bmatrix} \quad (1)$$

where, τ is the embedding delay, m is the embedding dimension, X indicates ionospheric clutter data at different range cells and x is time-domain sampling points and N is the total number of sampling points in X. Presuming there are L

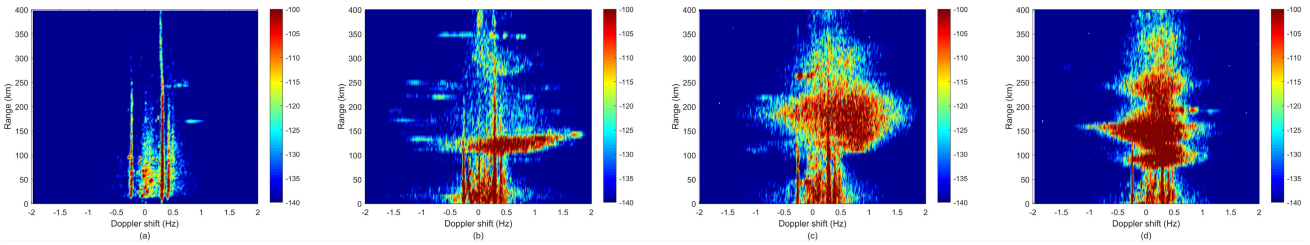

FIGURE 3. Range-Doppler spectrum from four sets of typical ionospheric clutter data: (a) simple E-layer and F-layer, (b) Expanding E-layer, (c) Expanding F-layer, (d) Expanding E-layer and expanding F-layer coexisting.

FIGURE 4. Transmitting antenna array and Receiving antenna array.

FIGURE 5. Remote and display system.

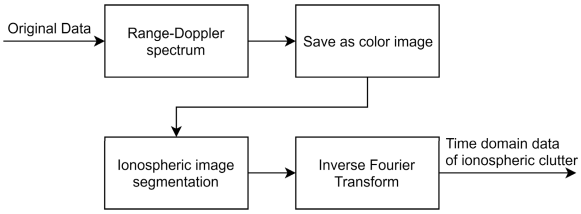

FIGURE 6. Ionospheric clutter extraction process.

range cells, and the experimental data is processed by pulse compression, the relationship about X, x and L is shown in Figure8.

III. INTRODUCTION TO CHAOTIC IDENTIFICATION METHODS

According to the phase-space reconstruction theorem, the phase diagram method, correlation dimension method and the largest Lyapunov exponent can be criteria for assessing the chaotic dynamics of ionospheric clutter in experimental time-series data.

A. PHASE DIAGRAM METHOD

The phase diagram of time series can describe the state varying in the nonlinear system and reflect the spatial structure of the attractor. If the trajectory of the phase-space attractor exhibits a state of non-periodic motion that the trajectory continuously extends and folds in a finite space, but it is not a repetitive motion of the periodic function, also it is different from random motion without regularity, then the system can be qualitatively determined as exhibiting chaotic characteristics. According to the particularity of ionospheric clutter in HFSWR, the phase diagram method can subjectively identify the chaotic dynamical characteristics of ionospheric clutter data.

B. SATURATED CORRELATION DIMENSION

The correlation dimension D_2 is the most intensely studied invariant quantity of the dynamic system. D_2 reflects the complexity of the attractors and in the chaotic dynamical process, D_2 has a fractal property. In addition, the strange attractor

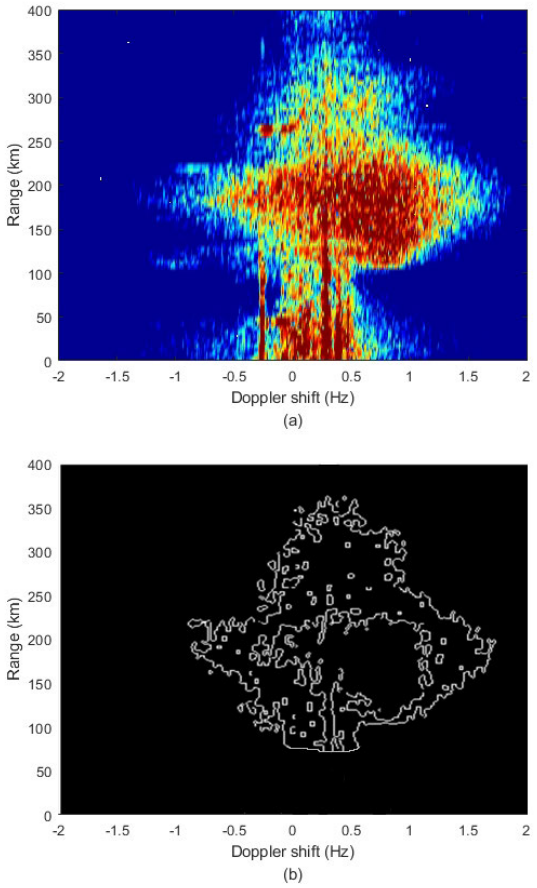

FIGURE 7. Ionospheric clutter extraction process: (a) the original ionospheric clutter data; (b) the outline of the ionospheric clutter in the R-D spectrum.

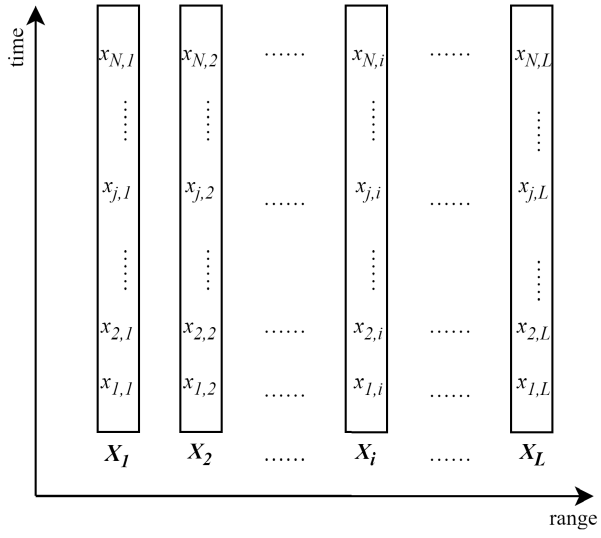

FIGURE 8. Radar data form.

is evidence of a chaotic process. The algorithm developed by Grassberger and Procaccia(GP) [22] is conceivably the most widely used for computing D2. Firstly, defining the correlation integral $C(r)$:

$$C(r) = \frac{1}{N(N-1)} \sum_{i=1}^{N} \sum_{j=1}^{N} \theta\left(r - \left\|X_i - X_j\right\|\right) \tag{2}$$

where, θ is the Heaviside function:

$$\theta(x) = \begin{cases} 0, & x \leq 0 \\ 1, & x > 0 \end{cases} \tag{3}$$

And $\left\|X_i - X_j\right\|$ is the distance between two points, the meaning of $C(r)$ is the proportion of pairs (distance between two points less than r) in all points. When $r \to 0$, $C(r)$ and r obeys the following law:

$$\lim_{r \to 0} C(r) \approx r^{D_2} \tag{4}$$

where, D_2 is the correlation dimension, it can be expressed as:

$$D_2 = \ln C_r / \ln r \tag{5}$$

For the chaotic time series, correlation integral $C(r)$ decays in exponential form, and the correlation dimension $C(r)$, which is taken as the power exponent of the correlation integral, gradually becomes stable, with the embedded dimension m increasing. Therefore, the saturation of the correlation dimension can be used as the criterion for judging the chaotic dynamical process of ionospheric clutter time-series data [23].

C. LARGEST LYAPUNOV EXPONENT

It has been confirmed that whether the largest Lyapunov exponent is exceeding zero can be an important characteristics in distinguishing strange attractors from ordinary attractors, which is also the criterion for the judgement of chaotic processes [24]. According to the definition of the Lyapunov exponent:

$$|\delta x(t_n)| = |\delta x(t_0)| \prod_{i=0}^{n-1} |f[x(t_i)]| = |\delta x(t_0)| e^{\lambda t_n} \tag{6}$$

where, $|\delta x(t_0)|$ is initial distance between two points, and $|\delta x(t_n)|$ is the new distance after n-iterations. Note:

$$\lambda = \lim_{t_n \to \infty} \frac{1}{t_n} \sum_{i=0}^{n-1} \ln |f[x(t_i)]| \tag{7}$$

where, τ is called the Lyapunov exponent, which reflects the sensitivity of the dynamic behavior of the system in comparison with the initial value over time. The largest positive Lyapunov exponent reflects that the time series has chaotic characteristics; the largest negative Lyapunov exponent indicates that the time series is random or periodic. The larger the Lyapunov exponent is, the more sensitive it is to the initial value. In the present study, the Wolf algorithm is selected to estimate the largest Lyapunov exponent, which is widely used in chaotic system research. All three aforementioned methods are based on phase-space reconstruction, which depends on the selection of the embedding dimension m and the delay

time τ. Varying values of m and τ may lead to different results, particularly when the experimental database contains a substantial amount of noise. Thereafter, two additional identification methods were selected, removing the necessity for phase-space reconstruction, namely, the power spectrum analysis method and the 0-1 test for chaos.

D. POWER SPECTRUM METHOD

The actual experimental time-series ionospheric clutter $X(t)$ exhibits the following spectrum $F(\omega)$:

$$F(\omega) = \int X(t) e^{i\omega t} dt \tag{8}$$

The corresponding power spectral density function $S(\omega)$ is:

$$S(\omega) = \frac{1}{T} |F(\omega)|^2 \tag{9}$$

Concerning the periodic or quasi-periodic motion systems, the power spectrum is a straight line or a narrow peak pulse. With reference to random noise, the power spectrum is a continuous curve of approximate level and for a chaotic process, the power spectrum is a continuous curve with an oscillation decline. Principally, the power spectrum method can identify and distinguish the chaotic dynamical process, periodic motions and random noises from the unique characteristics of time series in the time-frequency domain.

E. 0-1 TEST FOR CHAOS

The 0-1 test for chaos for deterministic dynamical systems is designed to distinguish between regular, periodic or quasi-periodic, and chaotic dynamics. It functions directly with the time series and does not require any phase-space reconstruction which needs to estimate the time delay and the embedding dimension. The 0-1 test for chaos analyses time series data directly without data preprocessing. Presuming that discrete ionospheric clutter time-series $X(t)$ with sampling time $t = 1, 2, \ldots, N$, and c is the random constant on the domain $(0, 2\pi)$, the define function $p(n)$ and $q(n)$ are:

$$p(n) = \sum_{t=1}^{n} X(t) \cos(\theta(t)), \quad n = 1, 2, \ldots, N \tag{10}$$

$$q(n) = \sum_{t=1}^{n} X(t) \sin(\theta(t)), \quad n = 1, 2, \ldots, N \tag{11}$$

where,

$$\theta(t) = t + c + \sum_{i=1}^{t} X(i), \quad t = 1, 2, \ldots, n \tag{12}$$

Based on function $p(n)$ and $q(n)$, define mean square displacement $M(n)$ is:

$$M(n) = M_c(n) - (E(X))^2 \times ((1 - \cos nc)/(1 - \cos c)) \tag{13}$$

where,

$$M_c(n) = \lim_{N\to\infty} \sum_{t=1}^{N} [(p(t+n) - p(j))^2 - (q(t+n) - q(t))^2] \tag{14}$$

and

$$E(X) = \lim_{N\to\infty} \frac{1}{N} \sum_{t=1}^{N} X(t) \tag{15}$$

Defining the asymptotic growth of $M(n)$ is K_c :

$$K_c = \lim_{n\to\infty} \lg M(n) \big/ \lg n \tag{16}$$

If $K_c \approx 1$, the ionospheric clutter is a chaotic process.

IV. EXPERIMENT RESULTS

In this section, the first stage requires a separation of ionospheric clutter from sea clutter and other noise according to the method depicted in Section II. Subsequently, the chaotic identification methods in Section IV were applied to process the actual experimental data. A comparison and analysis of the results produced by the different methods will now be presented.

A. IONOSPHERIC CLUTTER DATA PROCESSING

The radar echo signal of HFSWR is primarily composed of sea clutter, ionospheric clutter and other noise as shown in Figure2(a) to (d). According to Barrick [25] sea clutter Bragg theorem, the time-domain echo signal from sea clutter will peak at a specific frequency after pulse compression and the Fourier transform. In addition, the range cells occupied by ionospheric and sea clutter are different in Rang-Doppler spectrum, which indicates that the ionospheric clutter exists 90 kilometers away from the receiver, generally. Therefore, using the particular properties between two types of echo signals in the Range-Doppler spectrum, and then using the boundary abstraction method to track the location of the ionospheric clutter. The time-domain data of ionospheric clutter is obtained after an inverse Fourier transform. Finally, the data is subjected to filtering with a 102-tap FIR filter designed for concealing the high-frequency burrs. Four typical sets of ionospheric clutter data including E-layer clutter, F-layer clutter, expanding E-layer and expanding F-layer clutter, are selected in this experiment. Figure9(a) refers to unfiltered F-layer data, whilst Figure9(b) refers to the corresponding filtered data, and the additional three sets are processed in the same way, respectively.

B. PHASE-SPACE RECONSTRUCTION

The phase diagram method, the saturated correlation dimension and the largest Lyapunov exponent are all centered on the phase-space reconstruction, where the most important aspect is to estimate the time delay τ and the embedding dimension m. There are numerous alternative methods available to estimate τ and m. Thus, the mutual information(MI) [26] and false nearest neighbor(FNN) [27] method can be selected as they are proven to be effective and practical. The MI of $X(t)$ and $X(t+\tau)$ is defined as $I(\tau)$:

$$\begin{aligned} I(\tau) &= \sum P(X(t), X(t+\tau)) \\ &= \log_2 \left[\frac{P(X(t), X(t+\tau))}{P(X(t)) P(X(t+\tau))} \right] \end{aligned} \tag{17}$$

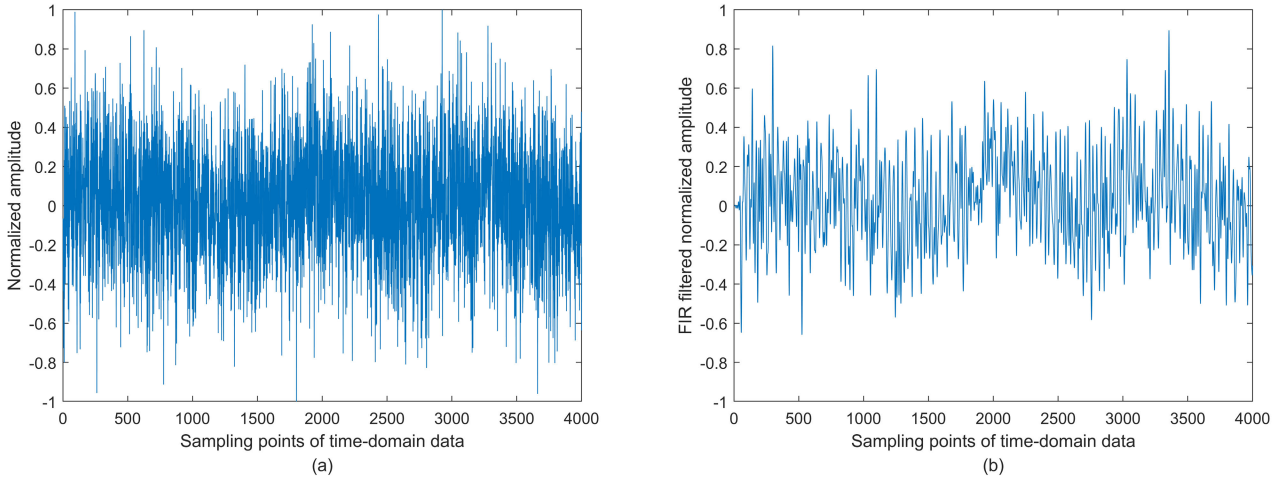

FIGURE 9. An example of time domain data from ionospheric F-layer clutter: (a) unfiltered F-layer time domain data, (b) filtered F-layer time domain data with FIR.

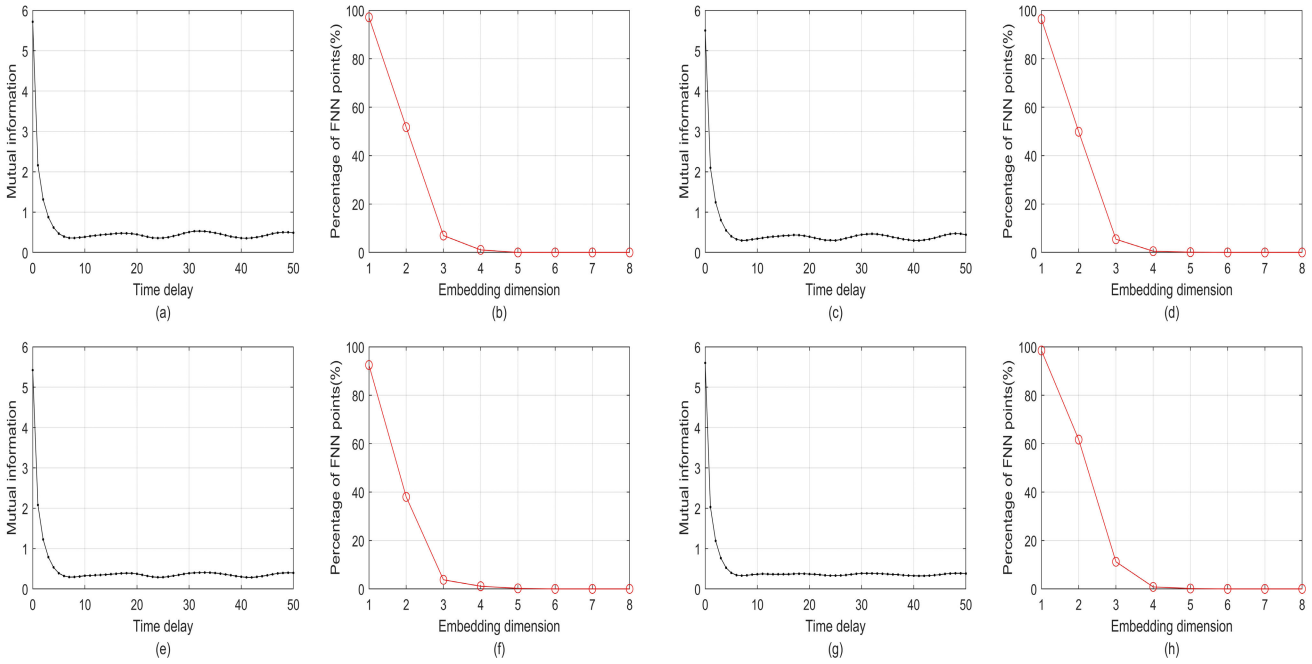

FIGURE 10. MI plots and FNN plots of typical ionospheric clutter data: (a) MI of E-layer data, (b) FNN of the same E-layer data, (c) MI of F-layer data, (d) FNN of the same F-layer data, (e) MI of expanding E-layer data, (f) FNN of the same expanding E-layer data, (g) MI of expanding F-layer data, (h) FNN of expanding F-layer data.

where $P(X(t))$ and $P(X(t+\tau))$ are normalized distribution functions of $X(t)$ and $X(t+\tau)$, and $P(X(t))P(X(t+\tau))$ is the joint probability distribution. The first minimum of the MI plot is selected as the embedding delay τ. Concerning the FNN method, presuming $X(t) = x(t), x(t+\tau), \ldots, x(t+(m-1)\tau)$, and $X_F(t)$ is the nearest neighbor point of $X(t)$, the distance between these two points is $R_m(t) = \|X(t) - X_F(t)\|$. Once the dimension of the phase space increases from m to $m+1$, the distance between the two points changes:

$$R_{m+1}^2(t) = R_m^2(t) + \|X(t+m\tau) - X_F(t+m\tau)\|^2 \quad (18)$$

Defining:

$$S_m = \frac{\|X(t+m\tau) - X_F(t+m\tau)\|}{R_m(t)} \quad (19)$$

If $S_m > S_r$, $X_F(t)$ is the FNN point of $X(t)$, where S_r is usually located in $(10, 50)$. In the event that the number of

FNN points decreases to zero or down to 5% stably with the embedding dimension increasing, m is referred to as the optimum embedding dimension. The time delay and embedding dimension of four sets of specific ionospheric clutter data are shown in Figure10. It can be observed from the Figure10(a), 10(c),10(e) and 10(g), that the time delay τ is approximately 8 or 9, where the plot reaches a minimum for the first time. Figure10(b), 10(d),10(f) and 10(h) indicate that the percentage of FNN points decreases with the embedding dimension. The optimum value is found to be 5 for four typical data sets. The MI method and FNN methods are repeated in each database sourced from HFSWR for the purpose of research, and the results are identical.

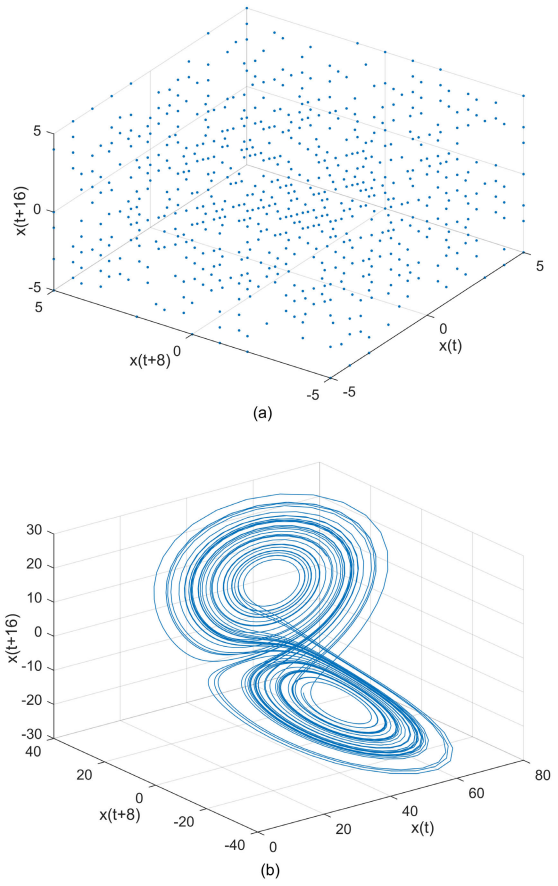

FIGURE 11. Typical phase diagram of random series and chaotic series: (a) phase diagram of random white noise,(b)phase diagram of Lorenz system.

C. PHASE DIAGRAM METHOD

The phase points of random time series are uniformly distributed in three-dimension spaces in Figure11(a). However, the chaotic dynamical process has a strange attractor and the phase points in three-dimension construct a special shape, resembling the attractor of the Lorenz [26] system which appears as a butterfly when plotted in Figure11(b).

According to the Equation (1), we can draw the attractor in the three-dimension space, by taking $N = 3$ and $\tau = 8$ obtained from the MI method. And the formula of the attractor is shown as:

$$R^m = \begin{bmatrix} X_1 \\ X_2 \\ X_{3+(m-1)\times 8} \end{bmatrix} = \begin{bmatrix} x_1 & x_{1+8} & \cdots & x_{1+(m-1)\times 8} \\ x_2 & x_{2+8} & \cdots & x_{2+(m-1)\times 8} \\ x_3 & x_{3+8} & \cdots & x_{3+(m-1)\times 8} \end{bmatrix} \quad (20)$$

The Figure12(a) to (d) indicate the phase diagram of E-layer, F-layer, expanding E- and F-layer ionospheric clutter data using the coordinated delay method with time delay. It can be observed from Figure12 that different types of ionospheric clutter data possess similar attractors, which all have a ''funnel'' shape, but not uniformly distributed in three-dimension. Thus, this provides the preliminary evidence that the ionospheric clutter is also a chaotic process.

D. SATURATED CORRELATION DIMENSION

The algorithm of estimating the correlation dimension D_2 is illustrated earlier in Section X. The typical result of a set of ionospheric clutter data is as shown in Figure13. The results from repeating this method to obtain 50 sets of ionospheric data indicate that the correlation dimension from different data sets is approximately 4.5 to 4.8, with the embedding dimension increasing from 2 to 30. Consequently, the saturated correlation dimension method can be used to determine the ionospheric time series with recognizable chaotic characteristics.

In this experiment, ionospheric clutter from expanding E- and F-layer exist between 100 to 300 kilometers, therefore, the results of ionospheric clutter from different range cells are presented in Table2.

TABLE 2. Estimated results of correlation dimension.

Range	E-layer	F-layer	Expanding E-layer	Expanding F-layer
100	-	-	4.682	-
130	-	-	4.757	-
160	4.536	-	4.732	-
190	-	-	4.665	-
210	-	-	-	4.725
240	-	4.584	-	4.747
270	-	-	-	4.775
300	-	-	-	4.802

Figure14 displays a graphical representation of the relationship between D_2 (only from the expanding E- and F-layer) and the ionospheric height.The correlation dimension is affected by height variation, and the plotted trends are similar to the electron density curve in Figure14(c), which indicates that the correlation dimension is relative to electron density.

E. LARGEST LYAPUNOV EXPONENT

As stated, Lyapunov exponents indicates how the trajectories of the attractor adjust under the evolution of dynamics, and the reciprocal of largest Lyapunov exponent is also the

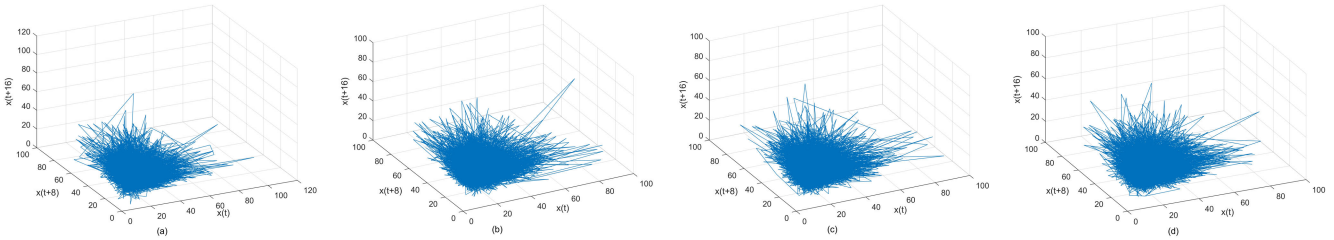

FIGURE 12. Attractors by coordinate time delay method in 3-dimension: (a) attractor of E-layer data, (b) attractor of F-layer data, (c) attractor of expanding E-layer data, (d) attractor of expanding F-layer data.

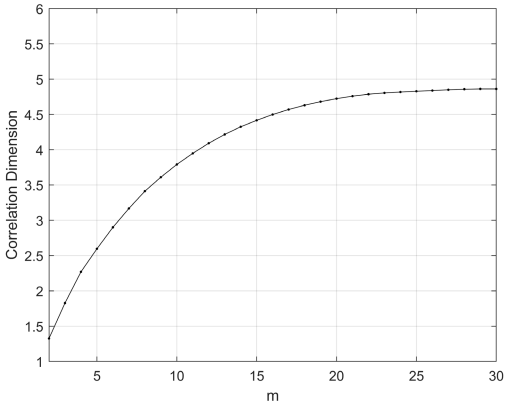

FIGURE 13. Correlation dimension of a set of typical ionospheric clutter data.

TABLE 3. Estimated results of largest Lyapunov exponent.

Range	E-layer	F-layer	Expanding E-layer	Expanding F-layer
100	-	-	0.223	-
130	-	-	0.224	-
160	0.205	-	0.235	-
190	-	-	0.241	-
210	-	-	-	0.242
240	-	0.210	-	0.250
270	-	-	-	0.268
300	-	-	-	0.277

longest predictable time of a chaotic process, which suggests that the greater the largest Lyapunov exponent is, the more difficult it is to predict. The Table3 displays the results of the estimated largest Lyapunov exponents of ionospheric clutter data, in correlation with the data in the previous section, according to the Wolf algorithm.

The Table3 suggests that the largest Lyapunov exponents are positive, and the estimated values range from approximately 0.200 to 0.280, which can confirm the chaotic feature of ionospheric clutter. The relationship between the largest Lyapunov exponent and ionospheric height is displayed in Figure15. Figure15 indicates that the largest Lyapunov exponent of F-layer exceeds that of E-layer, and the trend of the largest Lyapunov exponent plots increases as the height escalates.

According to Figure15(c), at height ranging from 100 to 300 kilometers, the temperature of the ionosphere elevates gradually. Higher temperatures lead to more intense electronic motion, which renders it more difficult to predict the changes of ionosphere, therefore, the largest Lyapunov exponent becomes greater with augmented height and temperature.

F. POWER SPECTRUM METHOD

The three aforementioned identification methods are associated with the phase-space reconstruction, and how the verification method has changed. It is apparent that a power spectrum density function curve with oscillatory descent is a necessary condition for a chaotic process. Figure16(a) to (d) present the power spectrum density function curves of four typical sets of ionospheric clutter data, and the trend of four curves is similar.

The graphs of the power spectrum of ionospheric clutter indicate that the dynamical system of ionospheric clutter has a dissipative structure. It is distinct from the peak pulse power spectrum of periodic motion and the horizontal fluctuation power spectrum of random noise.Therefore, the chaotic feature of ionospheric clutter time-series data can also be qualitatively determined by power spectrum analysis.

G. THE 0-1 TEST FOR CHAOS

In a regular system (periodic or quasiperiodic dynamics), the trajectories of the phase diagram of $p(n)$ and $q(n)$ are typically bound, whilst for a chaotic system, the trajectories typically exhibit a two-dimensional Brownian motion with zero drift [28]. For example, a logistic map is a type of chaotic process which has been studied extensively at present:

$$x_{n+1} = \lambda x_n (1 - x_n), \quad n = 1, 2, \ldots \tag{21}$$

where $0 \leq x \leq 1$ and $0 \leq \lambda \leq 4$.The value of λ determines whether the logistic system is chaotic. When $0 < \lambda \leq 1$, the system function has only one regular solution zero; when $1 < \lambda \leq 3$, the system function has two regular solution zero and $1 - 1/\lambda$, and when $3 < \lambda \leq 4$, the system gradually transforms from period doubling bifurcation into chaotic series. Figure17(a) shows the relationship between x and λ when $3 < \lambda \leq 4$. Figure17(b) and (c) show the 0-1 test for chaos using the logistic map data.

Similarly, the 0-1 test for chaos is repeated to determine the chaotic dynamics of the entire ionospheric database obtained from HFSWR. The plots of $p(n)$ and $q(n)$ from four typical data sets of E-layer, F-layer, expanding E- and F-layer are

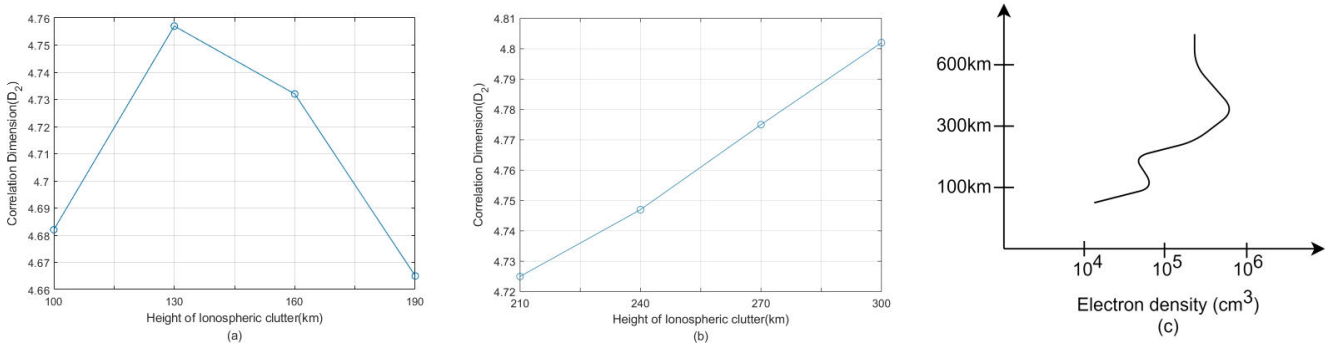

FIGURE 14. Relationship between correlation dimension and height: (a) correlation dimension and ionospheric height in expanding E-layer, (b) correlation dimension and ionospheric height in expanding F-layer, (c) ionospheric electron density and height.

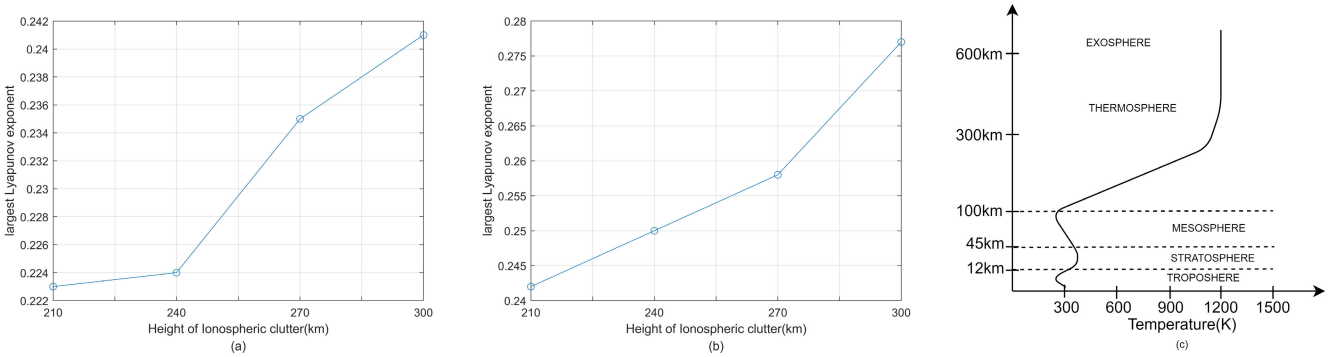

FIGURE 15. Relationship between largest Lyapunov exponent and ionospheric height: (a) largest Lyapunov exponent and ionospheric height in expanding E-layer, (b) largest Lyapunov exponent and ionospheric height in expanding F-layer.

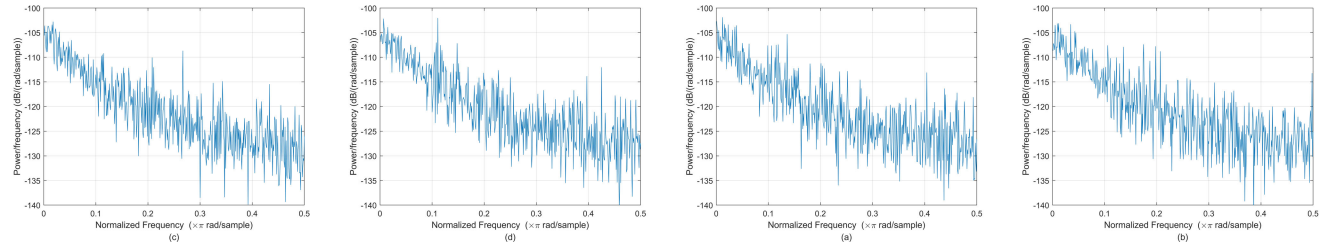

FIGURE 16. Typical power spectrum: (a) power spectrum of E-layer data, (b) power spectrum of F-layer, (c) power spectrum of expanding E-layer, (d) power spectrum of expanding F-layer.

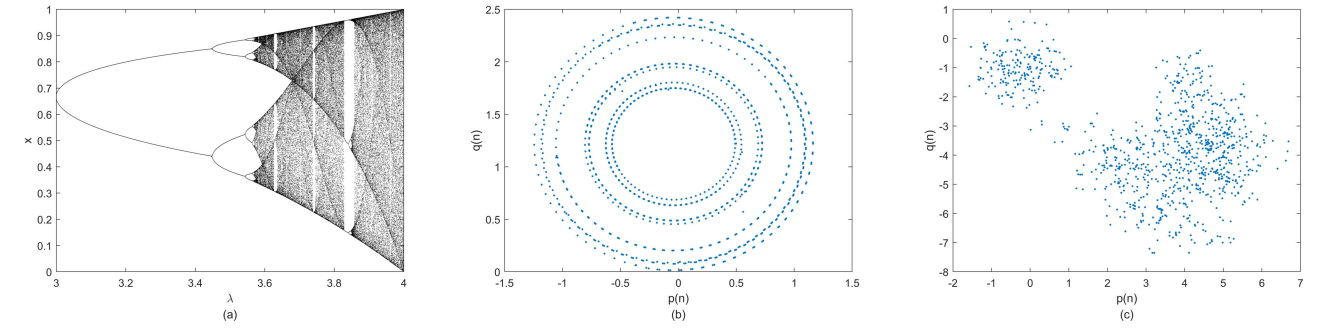

FIGURE 17. 0-1 test for Logistic map: (a) Bifurcation diagram of Logistic map, (b) $p(n)$ and $q(n)$ plot when $\lambda = 2.55$, (c) $p(n)$ and $q(n)$ plot when $\lambda = 3.55$.

shown in Figure18(a) to (d). In four typical cases, the plots exhibit a two-dimensional Brownian motion, similar to the logistic map when $3 < \lambda \leq 4$.

Furthermore, the values for asymptotic growth K_c estimated from different heights of ionospheric clutter are shown in Table4, where asymptotic growth K_c is not dependent on

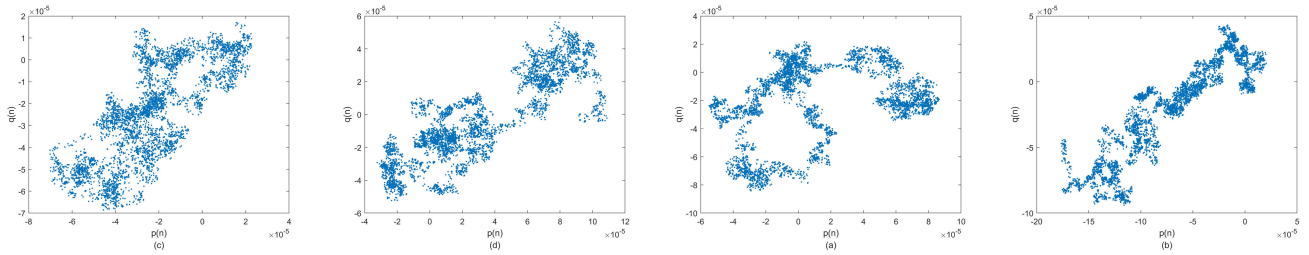

FIGURE 18. $p(n)$ and $q(n)$ plot :(a) $p(n)$ and $q(n)$ plot in E-layer data, (b) $p(n)$ and $q(n)$ plot in F-layer data, (c) $p(n)$ and $q(n)$ plot in expanding E-layer data, (d) $p(n)$ and $q(n)$ plot in expanding F-layer data.

TABLE 4. Estimated results of largest Lyapunov exponent.

Range	E-layer	F-layer	Expanding E-layer	Expanding F-layer
100	-	-	0.9981	-
130	-	-	0.9706	-
160	0.9876	-	0.9923	-
190	-	-	0.9871	-
210	-	-	-	0.9892
240	-	09626	-	0.9865
270	-	-	-	0.9733
300	-	-	-	0.9921

the ionospheric heights and each result is approximately 1. According to the $p(n)$ and $q(n)$ coordinates and asymptotic growth K_c, it can be assumed that the ionospheric clutter exhibits chaotic features once again.

V. CONCLUSION

The present study is the first to demonstrate that the ionospheric clutter of HFSWR is a chaotic dynamical process according to the comparison of five identification methods, namely phase diagram reconstruction, saturated correlation dimension, largest Lyapunov exponent analysis, plot of power spectrum and the 0-1 test for chaos. The experimental data consists of authentic measured experimental data from HFSWR. Moreover, throughout the procedure of data processing, several additional significant characteristics of ionospheric clutter were discovered:

1) The ionospheric clutter in HFSWR has chaotic features, which [is/are] independent of ionosphere expansion in the Range-Doppler spectrum.
2) The time delay of ionospheric clutter is approximately 8 or 9 and the embedding dimension is 5.
3) The correlation dimension D2 of ionospheric clutter is in the range of 4.5-4.9, less than the embedding dimension. In addition, the correlation dimension has positive relevance with the electron density.

It is worth studying the chaotic dynamics of ionospheric clutter in HFSWR. At present, chaotic nonlinear analysis methods can be used to process the signals. Subsequently, the predicted model of ionospheric clutter in HFSWR will be established and this chaotic dynamical model may help to suppress the ionospheric clutter for ultimately improving high-frequency radar detection performance.

REFERENCES

[1] F. Jangal, S. Saillant, and M. Hélier, "Wavelet contribution to remote sensing of the sea and target detection for a high-frequency surface wave radar," *IEEE Geosci. Remote Sens. Lett.*, vol. 5, no. 3, pp. 552–556, Jul. 2008.

[2] D. Barrick, "First-order theory and analysis of MF/HF/VHF scatter from the sea," *IEEE Trans. Antennas Propag.*, vol. AP-20, no. 1, pp. 2–10, Jan. 1972.

[3] D. Barrick, "History, present status, and future directions of HF surface-wave radars in the U.S." in *Proc. Int. Conf. Radar*, 2003, pp. 652–655.

[4] W. Wang and L. R. Wyatt, "Radio frequency interference cancellation for sea-state remote sensing by high-frequency radar," *IET Radar, Sonar Navigat.*, vol. 5, no. 4, pp. 405–415, Feb. 2010.

[5] Y. T. Liu, R. Q. Xu, and N. Zhang, "Progress in HFSWR research at harbin Institute of technology," in *Proc. Int. Conf. Radar*, Adelaide, SA, Australia, Sep. 2003, pp. 522–528.

[6] H. C. Chan, "Characterization of ionospheric clutter in HF surface-wave radar," *Defence R&D Canada-Ottawa*, vol. 13, no. 12, pp. 10–25, 2003.

[7] J. Wei, D. Weibo, and S. Jialin, "Characteristic study of ionospheric clutter in high-frequency over the horizon surface wave radar," in *Proc. IEEE Youth Conf. Inf., Comput. Telecommun.*, Sep. 2009, vol. 1, no. 2, pp. 154–157.

[8] H. Gao, G. Li, Y. Li, Z. Yang, and X. Wu, "Ionospheric effect of HF surface wave over-the-horizon radar," *Radio Sci.*, vol. 41, no. 6, pp. 102–112, 2006.

[9] S. Chen, W. Huang, and E. W. Gill, "A vertical reflection ionospheric clutter model for HF radar used in coastal remote sensing," *IEEE Antennas Wireless Propag. Lett.*, vol. 14, pp. 1689–1693, 2015.

[10] J. Walsh, E. W. Gill, W. Huang, and S. Chen, "On the development of a high-frequency radar cross section model for mixed path ionosphere–ocean propagation," *IEEE Trans. Antennas Propag.*, vol. 63, no. 6, pp. 2655–2664, Jun. 2015.

[11] J. Walsh, S. Chen, E. Gill, and W. Huang, "High frequency radar clutter power for mixed ionosphere-ocean propagation," in *Proc. 16th Int. Symp. Antenna Technol. Appl. Electromagn.*, Jul. 2014, pp. 1–2.

[12] W. John, W. M. Huang, and E. W. Gill, "An analytical model for HF radar ionospheric clutter," in *Proc. IEEE Antennas Propag. Soc. Int. Symp. (APSURSI)*, Jul. 2013, pp. 1974–1975.

[13] R. Maryam and R. S. Adve, "Ionospheric clutter model for high frequency surface wave radar," in *Proc. IEEE Radar Conf.*, May 2012, pp. 377–382.

[14] M. Ravan, R. J. Riddolls, and R. S. Adve, "Ionospheric and auroral clutter models for HF surface wave and over-the-horizon radar systems," *Radio Sci.*, vol. 47, no. 3, pp. 1–12, 2012.

[15] Y. Li, Y. Wei, R. Xu, Z. Wang, and T. Chu, "An ionospheric Es layer clutter model and suppression in HF surfacewave radar," *Int. J. Antennas Propag.*, vol. 2013, May 2013, Art. no. 320645.

[16] T. Wen-Long, L. Gao-Peng, and X. Rong-Qing, "Ionospheric clutter mitigation for high-frequency surface-wave radar using two-dimensional array and beam space processing," *IET Radar, Sonar Navigat.*, vol. 6, no. 3, pp. 202–211, Mar. 2012.

[17] M. Wu, B. Y. Wen, and H. Zhou, "Ionospheric clutter suppression in HF surface wave radar," *J. Electromagn. Waves Appl.*, vol. 23, no. 10, pp. 1265–1272, 2009.

[18] F. Jangal, S. Saillant, and M. Hélier, "Ionospheric clutter mitigation using one-dimensional or two-dimensional wavelet processing," *IET Radar, Sonar Navigat.*, vol. 3, no. 2, pp. 112–121, Apr. 2009.

[19] H. Zhou, B. Wen, and S. Wu, "Ionosphere probing with a high frequency surface wave radar," *Prog. Electromagn. Res. C*, vol. 20, no. 1, pp. 203–214, 2011.
[20] S. Chen, "Ionospheric clutter models for high frequency surface wave radar," Ph.D. dissertation, Dept. Elect. Comput. Eng., Memorial Univ. Newfoundland, St. John's, NL, Canada, 2012, vol. 1, no. 1, pp. 102–112.
[21] F. Takens, "Detecting strange attractors in turbulence," in *Dynamical Systems and Turbulence, Warwick 1980* (Lecture Notes in Mathematics), vol. 898, D. A. Rand and L.-S. Young, Eds. Groningen, The Netherlands: Mathematics Institute, 1980, pp. 366–381.
[22] P. Grassberger and I. Procaccia, "Estimation of the Kolmogorov entropy from a chaotic signal," *Phys. Rev. A, Gen. Phys.*, vol. 28, no. 4, p. 2591, 1983.
[23] A. Wolf, J. B. Swift, H. L. Swinney, and J. A. Vastano, "Determining Lyapunov exponents from a time series," *Phys. D, Nonlinear Phenomena*, vol. 16, no. 3, pp. 285–317, 1985.
[24] P. Hanchuan, F. Long, and C. Ding, "Feature selection based on mutual information criteria of max-dependency, max-relevance, and min-redundancy," *IEEE Trans. Pattern Anal. Mach. Intell.*, vol. 8, no. 8, pp. 1226–1238, Aug. 2005.
[25] H. D. I. Abarbanel and M. B. Kennel, "Local false nearest neighbors and dynamical dimensions from observed chaotic data," *Phys. Rev. E, Stat. Phys. Plasmas Fluids Relat. Interdiscip. Top.*, vol. 47, no. 5, p. 3057, 1993.
[26] G. A. Leonov, N. V. Kuznetsov, N. A. Korzhemanova, and D. V. Kusakin, "Lyapunov dimension formula for the global attractor of the Lorenz system," *Commun. Nonlinear Sci. Numer. Simul.*, vol. 41, pp. 84–103, Dec. 2016.
[27] K. G. Budden, "Radio waves in the ionosphere," in *Radio Waves in the Ionosphere*, K. G. Budden, Ed. Cambridge, U.K.: Cambridge Univ. Press, 2009.
[28] G. A. Geory and I. Melbourne, "A new test for chaos in deterministic systems," *Proc. Roy. Soc. London, Ser. A, Math., Phys. Eng. Sci.*, vol. 460, pp. 603–611, Feb. 2004.

LYU ZHE received the B.Sc. degree in electronic information engineering and the M.Sc. degree in electronics and information engineering from the Harbin Institute of Technology, China, in 2013 and 2017, respectively, where he is currently pursuing the Ph.D. degree in information and communication engineering. His research interests include ionosphere remote sensing, clutter suppression, signal prediction, and radar signal processing.

YU CHANGJUN received the B.S. degree in electronic engineering from the Harbin Institute Technology, Harbin, China, in 1984, and the M.S. and Ph.D. degrees in information and communication engineering from Harbin Engineering University, Harbin, in 1990 and 2010, respectively. He is currently a Professor with the School of Information and Electrical Engineering, Harbin Institute of Technology at Weihai, Weihai, China. His research interests include high-frequency surface wave radar (HFSWR) system design and analysis, target detection, estimation and tracing, and ionosphere remote sensing.

LIU AIJUN received the B.S. and M.S. degrees in communication engineering and information and signal processing from Dalian Maritime University, Dalian, China, in 1995 and 2003, respectively, and the Ph.D. degree in information and communication engineering from the Harbin Institute of Technology, Harbin, China, in 2011. He is currently a Professor with the School of Information Science and Engineering, Harbin Institute of Technology at Weihai. His research interests include high-frequency surface wave radar system design and analysis, array signal processing, and signal time-frequency analysis.

YANG XUGUANG was born in Gansu, China, in 1984. He received the B.S. and M.S. degrees in mathematics from the Harbin Institute of Technology, Harbin, China, in 2005 and 2007, respectively. He is currently pursuing the Ph.D. degree in electronic engineering with the Harbin Institute of Technology, Harbin. From 2007 to 2018, he was an Assistant Professor with the College of Science, Harbin Engineering University, China. Since 2018, he has been an Associate Professor with the Mathematics Department. His research interests include the ocean and ionosphere remote sensing from high-frequency surface wave radar (HFSWR) spectra, and the reaction-diffusion equations with applications in pattern formations.

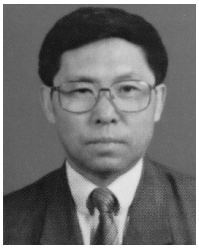

QUAN TAIFAN received the B.S. degree from the Department of Electrical Engineering, Tsinghua University, Beijing, China, in 1977, and the M.S. degree from the Department of Control Science and Engineering, Harbin Engineering University, Harbin, China, in 1983. He is currently a Professor with the College of Electronic and Information Engineering, Harbin Institute of Technology, Harbin, China. His research interests include high-frequency surface wave radar (HFSWR) system design and analysis, multisensor multitarget data fusion system, neural network, and joint remote sensing of sea state and ionosphere.